Aalborg Universitet

AALBORG UNIVERSITY
DENMARK

The interaction between the stratosphere and the troposphere as revealed by singular vectors

Hooghoudt, Jan Otto; Barkmeijer, Jan A N

Published in:
Meteorologische Zeitschrift

DOI (link to publication from Publisher):
10.1127/0941-2948/2007/0254

Creative Commons License
Unspecified

Publication date:
2007

Document Version
Publisher's PDF, also known as Version of record

Link to publication from Aalborg University

Citation for published version (APA):
Hooghoudt, J. O., & Barkmeijer, J. A. N. (2007). The interaction between the stratosphere and the troposphere as revealed by singular vectors. *Meteorologische Zeitschrift*, *16*(6), 723-739. https://doi.org/10.1127/0941-2948/2007/0254

General rights
Copyright and moral rights for the publications made accessible in the public portal are retained by the authors and/or other copyright owners and it is a condition of accessing publications that users recognise and abide by the legal requirements associated with these rights.

- Users may download and print one copy of any publication from the public portal for the purpose of private study or research.
- You may not further distribute the material or use it for any profit-making activity or commercial gain
- You may freely distribute the URL identifying the publication in the public portal -

Take down policy
If you believe that this document breaches copyright please contact us at vbn@aub.aau.dk providing details, and we will remove access to the work immediately and investigate your claim.

Meteorologische Zeitschrift, Vol. **16**, No. 6, 723-739 (December 2007)
© by Gebrüder Borntraeger 2007

Article

The interaction between the stratosphere and the troposphere as revealed by singular vectors

JAN-OTTO HOOGHOUDT* and JAN BARKMEIJER

Royal Netherlands Meteorological Institute (KNMI), De Bilt, Netherlands

(Manuscript received March 3, 2007; in revised form August 3, 2007; accepted August 23, 2007)

Abstract

Stratospheric singular vectors (S-SV's) have been calculated with one of the latest versions of the ECMWF model, for the months January and July 2004–2006. Basic properties as amplification, wavenumber spectra and preferred geographical position are studied. In January, the majority of these S-SV's amplify by growing on the background wind shear of the polar vortex. For July, the amplification of the S-SV's is mainly associated with the tropospheric summer jet, that extends above 100 hPa. The S-SV's are located lower (100 to 50 hPa) in the stratosphere than the January SV's and their amplification is less. We have also calculated S-SV's during the stratospheric sudden warming (SSW) of January 2006. The amplification factor of the S-SV's does not seem to be affected by the SSW. The breaking of the polar vortex is however clearly reflected in the preferred geographical location of the S-SV's. In addition to these 'pure' stratospheric SV's, perturbations have been calculated that initially are located in the stratosphere, but that are optimized to maximize the perturbation energy growth in the low troposphere (below 500 hPa) on a time scale of 48 and 120 hours. Basic properties of this type of SV's are studied. First results, for these Stratosphere-Troposphere SV's (ST-SV's), show that they mainly seem to rely on the tropospheric jet to maximize their amplification. From a non-modal point of view, small-scale structures with maximal amplitude around total wavenumber 10 seem to be important in the interaction between the stratosphere and troposphere.

Zusammenfassung

Stratosphärische Singuläre Vektoren (S-SVs) wurden mit einer der neuesten Versionen des ECMWF Modells für die Monate Januar und Juli 2004–2006 berechnet. Grundlegende Eigenschaften wie Amplifizierung, Wellenzahlspektren und bevorzugte geographische Lage wurden untersucht. Im Januar wird die Mehrheit dieser S-SVs durch ein Anwachsen der Hintergrundswindscherung des polaren Vortex verstärkt. Im Juli steht die Verstärkung der S-SVs vor allem im Zusammenhang mit dem troposphärischen Sommerstrahlstrom, der sich auf über 100 hPa erstreckt. Im Juli befinden sich die S-SVs niedriger (100 bis 50 hPa) in der Stratosphäre als im Januar und ihre Amplifizierung ist geringer. Darüber hinaus haben wir die S-SVs während der Plötzlichen Stratosphärischen Erwärmung (PSE) im Januar 2006 berechnet. Der Amplifizierungsfaktor der S-SVs scheint nicht durch die PSE beeinflusst zu sein. Das Aufbrechen des polaren Vortex spiegelt sich jedoch deutlich in der bevorzugten geographischen Lagen der S-SVs wider. Zusätzlich zu diesen "rein" stratosphärischen SVs wurden Störungen berechnet, die sich zunächst in der Stratosphäre befinden, aber optimiert wurden, um das Energiewachstum in der unteren Troposphäre (unterhalb von 500 hPa) über eine Zeitskala von 48 und 120 Stunden zu maximieren. Grundlegende Eigenschaften dieser Art von SVs werden untersucht. Erste Ergebnisse für diese Stratosphäre-Troposphäre-SVs (ST-SVs) zeigen, dass die Maximierung ihrer Amplifizierung sich in erster Linie nach dem troposphärischen Strahlstrom zu richten scheint. Von einem nicht-modalen Standpunkt aus gesehen, scheint es, dass klein-skalige Strukturen mit einer maximalen Amplitude im Bereich einer Gesamtwellenzahl von 10 eine wichtige Rolle im Zusammenspiel von Troposphäre und Stratosphäre spielen.

1 Introduction

By now, the idea that both the troposphere and the stratosphere play an important role in defining the atmospheric circulation is generally accepted. As a consequence, the vertical resolution of operational global circulation models (GCM's), has increased considerably over the last years. This has enabled, for example, performing data-assimilation over an atmospheric column extending well into the stratosphere (UPPALA et al., 2005; KALNAY et al., 1996).

Simultaneous with the operational use of these GCM's with increased vertical resolution, there is also need to investigate instability mechanisms which were formerly not well described by the model dynamics. This will be the subject of this paper. We want to explore the use of singular vectors (KALNAY, 2003) in gaining insight in the instability processes present in the stratosphere and in the interaction between the stratosphere and the troposphere. Over the years SV's have demonstrated their use, e.g. in ensemble forecasting, to inform about tropospheric instability processes. With the recent GCM versions, it becomes worthwhile to study, how the same technique behaves when con-

*Corresponding author: J.O. Hooghoudt, Royal Netherlands Meteorological Institute (KNMI), PO Box 201, 3730 AE De Bilt, The Netherlands, e-mail: otto.hooghoudt@knmi.nl

0941-2948/2007/0254 $ 7.65

DOI: 10.1127/0941-2948/2007/0254

© Gebrüder Borntraeger, Berlin, Stuttgart 2007

a)

Model level	Pressure (hPa)
1	0.1
15	12.3
20	35.8
22	54.6
25	96.0
30	202.1
39	500.0
60	1012.0

b)

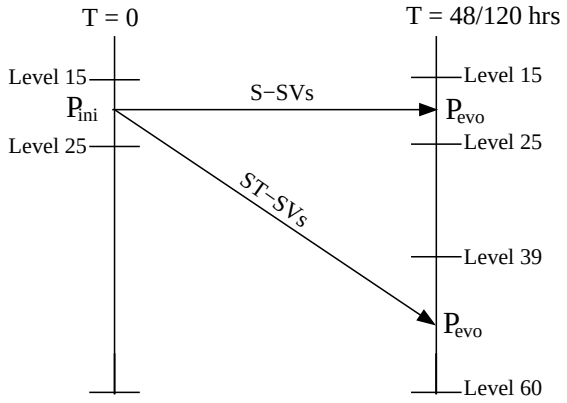

Figure 1: (a) Table showing the average pressure at some selected model levels (ml) of the ECMWF 60-layer model. (b) Schematic representation of the two SV configurations. P_{ini} and P_{evo} refer to the projection operators used at respectively, initial and final time.

fronted with stratospheric dynamics. It will also be interesting to see to what extent earlier results on stratospheric SV's (HARTMANN et al., 1996), obtained with a much coarser vertical resolution, remain valid. In this paper we will study the basic properties of these stratospheric SV's (S-SV's), such as spatial structure, wave number spectra, preferred geographical location and propagation speed.

Since highly nonlinear boundary layer and precipitation generating processes play no role in the stratosphere (HAYNES, 2005), it is very well possible that the linear approximation in the stratosphere is valid for longer forecast times than is the case for the troposphere. The results in JUNG and BARKMEIJER (2005) confirm this. Therefore, we have calculated S-SV's for two optimization time intervals (OTI's): 2 and 5 days.

Further, we have made a study of the SSW (O'NEILL, 2003; ANDREWS et al., 1987) that occurred in January 2006. We have studied to what extent the singular values and the preferred location of the S-SV's change during the SSW event.

The view that the stratosphere can have a direct influence on events in the troposphere is now widely accepted. This is mainly due to the pioneering research of BALDWIN and DUNKERTON (1999) and the research that their work initiated. Baldwin and Dunkerton showed, by using 40 years of daily data, that the largest amplitude anomalies in the lower stratospheric zonal flow (10 hPa) frequently appear to descend to tropospheric levels on a timescale of 3 weeks. The predictive skill associated with the downward propagation has been estimated by BALDWIN et al. (2003) and CHARLTON et al. (2003), by using statistical models. Both studies conclude that a small amount of extra skill (5 %) can be obtained in Northern Hemisphere weather on time scales of 10 to 45 days (see also e.g. CHRISTIANSEN, 2005).

In addition to these observational and statistical studies, also a variety of studies have been carried out by using numerical models of the atmosphere. The first among them was by BOVILLE (1984). In order to quantify the impact of inaccuracies in the stratosphere, he changed the stratospheric diffusion in his model. He found significant tropospheric changes as compared to his control run. The response closely resembled the spatial structure of the North Atlantic Oscillation (NAO).

Motivated by the aforementioned observational and model results together with the still missing, clear dynamical picture of how the stratosphere may be linked to the troposphere (SONG and ROBINSON, 2004), we have made a preliminary study to the possible role of linear non-modal perturbation growth (FARRELL and IOANNOU, 1996) in the stratosphere-troposphere interaction.

We have calculated those perturbations (ST-SV's) that are initially confined to the stratosphere and that are designed to give maximum linear perturbation growth in the lower (below 500 hPa) troposphere. As in the case of the S-SV's, we have computed ST-SV's with OTI's of 2 and 5 days.

By studying the basic properties of these 2-day and 5-day ST-SV's, we hope to gain insight in mechanisms which can optimally contribute to the interaction between stratosphere and troposphere.

2 Model and experiments

The forecast model we have employed in this study is a recent version of the ECMWF model, triangularly truncated at wavenumber 42 and with 60 levels in the vertical. For this configuration, the model extends well into the stratosphere with the highest level at 0.1 hPa (see F. 1a). In this paper we will use the following defining equation of the SV's:

$$E^{-1/2}P^*_{ini}\mathbf{M}^*P^*_{evo}EP_{evo}\mathbf{M}P_{ini}E^{-1/2}\mathbf{v}_i(0) = \sigma_i^2\mathbf{v}_i(0). \tag{2.1}$$

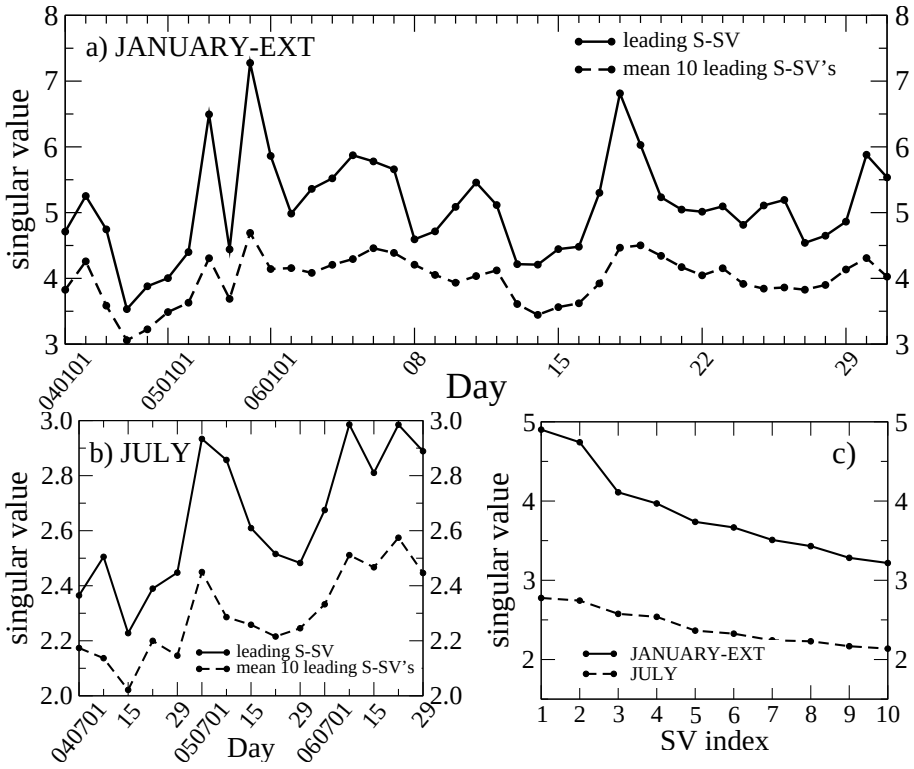

Figure 2: The leading singular value (solid line) and the mean singular value of the 10 leading S-SV's (dashed line) are displayed for (a) JANUARY-EXT, and (b) JULY. (c) Averaged singular value of the ten leading S-SV's as a function of their index, for JANUARY-EXT (solid) and JULY (dashed).

Nearly the same eigenvalue problem has to be solved for tropospheric SV's (see BUIZZA and PALMER, 1995); the difference is the use of projection operator P_{ini} and P_{evo} to which we come back later.

The components of the eigenvectors v_i comprise vorticity, divergence, temperature and logarithm of the surface pressure. The so-called forward propagator **M**, is the linear operator that describes the linear evolution of perturbations along the nonlinear trajectory from initial time $t_0 = 0$ to a future time t. The default OTI used in this paper is 48 hours; when different this will be explicitly mentioned. The projection operators P_{ini} and P_{evo} confine the region (horizontally as well as vertically) where a perturbation initially is located (P_{ini}) and where, at final time, perturbation energy is maximized (P_{evo}). We have used the total energy (TE) norm (ERRICO, 2000) as expressed by E and σ_i is the singular value corresponding to eigenvector $\mathbf{v}_i(0)$. The adjoint operators P^*_{ini}, P^*_{evo} and $\mathbf{M}^*$ are defined with respect to the Euclidean inner product The initial time structures $\{P_{ini}E^{-1/2}\mathbf{v}_i(0)\}_{i=1}^N$ and corresponding final time structures $\{P_{evo}\mathbf{M}P_{ini}E^{-1/2}\mathbf{v}_i(0)\}_{i=1}^N$ form a orthogonal set with respect to the total energy inner product.

The properties of the two types of SV's which will be studied in this paper are controlled by defining suitable vertical projection operators P_{ini} and P_{evo}. Because for now we are interested in processes in the extra-tropics, the P_{evo} we have used to calculate both types of SV's is a vertical projection as well as a horizontal projection. It projects onto the area north of 30°N. The operator P_{ini} does not include a horizontal projection. We can now distinguish the following two types of SV's:

- S-SV's (stratospheric SV's) start in the low stratosphere (between level 15–25) and produce maximal total energy perturbation growth in the same vertical zone. Here P_{ini} and P_{evo} are identical in the vertical and set the state-vector to zero outside the levels 15–25.

- ST-SV's (stratospheric-tropospheric SV's) also start in the low stratosphere (between level 15–25) but produce maximal perturbation total energy in the low troposphere (level 39–60). Here P_{ini} and P_{evo} set the state vector to zero outside the vertical zone of level 15–25 and level 39–60 respectively.

In appendix A.1 we explain why we have chosen level 15 and 25 as the lower and upper boundary for the P_{ini} projection operator.

For both experimental set-ups we have calculated the 10 leading SV's for 5 days in January (1, 8, 15, 22 and 29 January) and for 5 days in July (1, 8, 15, 22 and 29 July) for the years 2004, 2005 and 2006. We will refer to these two sets as 'JANUARY' and 'JULY', respectively. During January 2006 a SSW occurred. To investigate the S-SV and ST-SV properties under these circumstances,

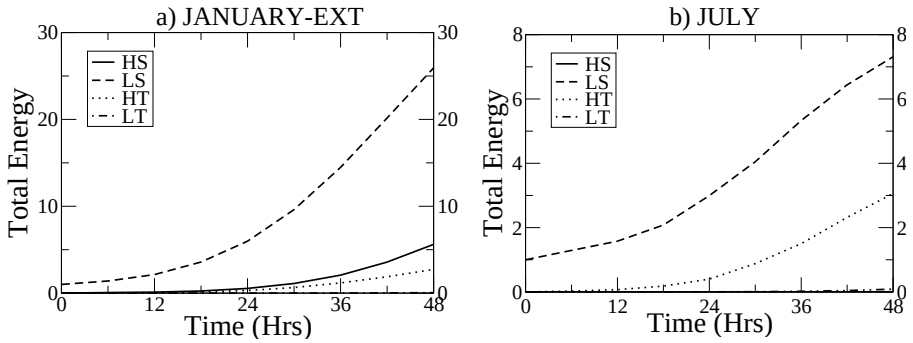

Figure 3: Average growth with time of total energy (kg, m^2s^{-2}) over 4 parts of the atmosphere: high stratosphere (solid), low stratosphere (dashed), high troposphere (dotted) and low troposphere (dashed-dotted), for the leading S-SV's of (a) JANUARY-EXT, and (b) JULY.

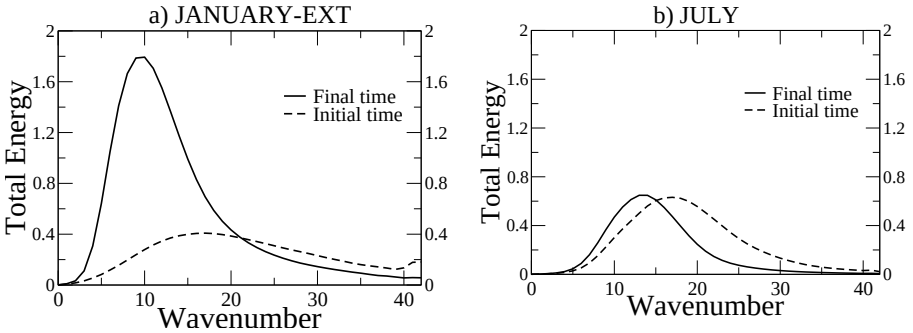

Figure 4: Total energy spectra in terms of total wavenumber for the 10 leading S-SV's of (a) JANUARY-EXT, and (b) JULY. Values at initial (final) time are dashed (solid). The total energy (kg, m^2s^{-2}) at initial time has been multiplied by a factor 10.

we have extended the SV computation to all 31 days of January 2006. This extended set (including the 5 days of January 2004 and 2005 and the 31 days of 2006), will be referred to as the 'extended January' set (JANUARY-EXT).

In the following two sections, we discuss the basic properties of respectively the S-SV's and the ST-SV's. In section 5 the similarity (BUIZZA, 1998) between ST-SV's with regular tropospheric SV's is shortly discussed. In section 6 the effect of the SSW in January 2006 on the singular values and preferred location of the S-SV's and ST-SV's is discussed. Concluding comments are given in section 7.

3 Stratospheric SV's

3.1 Amplification

In Fig. 2, the first singular value and the mean singular value of the ten leading S-SV's are displayed for JANUARY-EXT and for JULY. For JANUARY-EXT the leading singular value is on average 4.9, with extremes around 7. For JULY the leading singular value is on average 2.8, with the extremes reaching 3. In Fig. 2c the average singular values for JANUARY-EXT and JULY are shown as a function of their index.

When comparing the stratospheric singular values with the values found in the troposphere (see e.g. HOSKINS et al., 2000), we conclude that the singular values are around a factor 3 smaller in the stratosphere than in the troposphere.

In January the amplification is higher than in July, because of the higher background velocities (due to the polar vortex), associated with larger horizontal and vertical shears. The relation between the preferred location of the S-SV's and the background wind (shear) is discussed in section 3.3. The behavior of the S-SV's during the occurrence of a SSW is discussed in section 6.

3.2 Energy Distribution

To see how and where in the vertical column S-SV's amplify, we have divided the atmospheric column into four components: high stratosphere (level 1 to 14, HS), low stratosphere (level 15 to 25, LS), high troposphere (level 26 to 38, HT) and low troposphere (level 39 to 60, LT). Fig. 3a displays the growth of the total energy with time in these 4 parts of the atmosphere for the leading S-SV's of JANUARY-EXT. Although S-SV's are designed to maximize perturbation growth in the low stratosphere, growth at other vertical levels is still possible. From Fig. 3a we notice however, that most of the S-SV perturbation growth takes place in the low stratosphere, for which it was designed. At final time 76 % of the energy is in the LS and less then 0.2 % penetrates into the LT. For JULY (Fig. 3b), at final time, 70 % of the energy is in the LS and almost all the rest (29 %) is in the HT.

The main difference between JANUARY-EXT and JULY is that for JANUARY-EXT 16 % of the energy

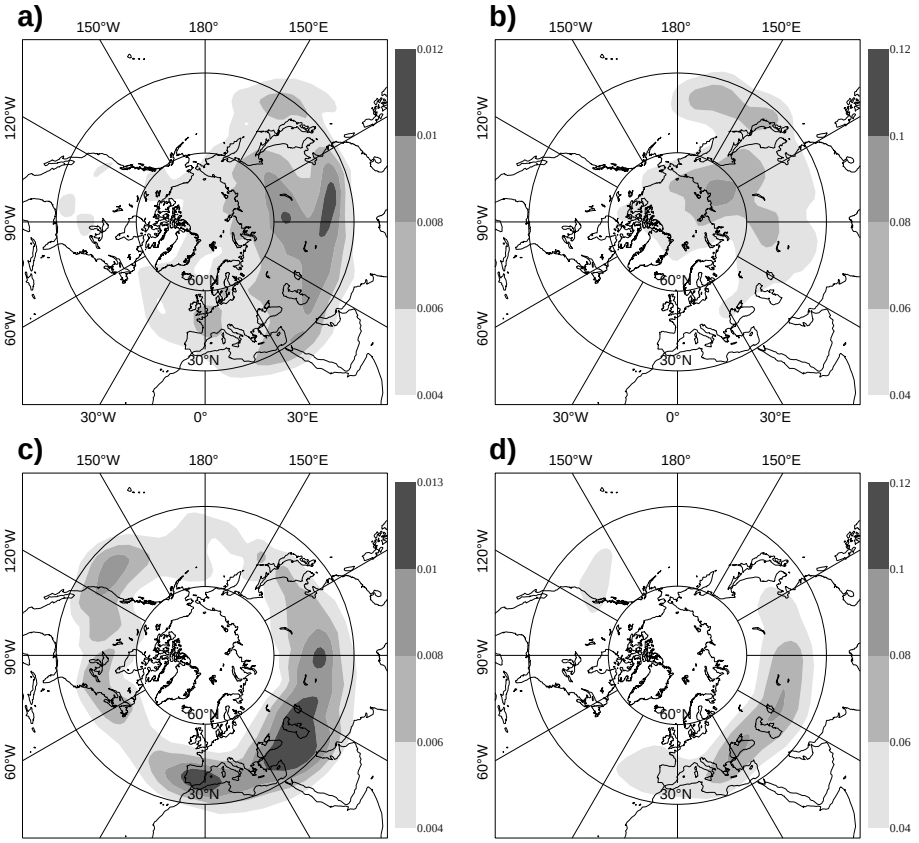

Figure 5: RMS of streamfunction (m^2s^{-1}) for the 10 leading S-SV's of the default JANUARY set at level 22 at (a) initial time, and (b) final time; (c,d) same as (a,b) but for JULY. Values have to be multiplied with 1.0 x 10^6 m^2s^{-1}. Notice that the values at final time are 10 times larger than at initial time.

at final time is found in the HS, while in JULY this is less then 1 %. So in July, there is no energy transport from the low to the high stratosphere.

Closer investigation of individual S-SV's, reveals that for JANUARY-EXT, initially, in around 30 % of the cases the total energy is distributed low in the LS. In the remainder of the cases, the S-SV's have their total energy maximum at level 18 (23 hPa). These latter S-SV's are responsible for the energy growth in the high stratosphere. For JULY all S-SV's are initially located in the lower part of the LS. These S-SV's do not give any growth in the HS during the forecast time. For an example of both cases see Fig. 7 and 8 in section 3.4.

For JANUARY-EXT and JULY, at initial time, the kinetic energy (KE) is on average responsible for respectively 40 % and 25 % of the total amount of total energy, and increases for both cases to 75 % at final time.

In Fig. 4 the total wavenumber spectra is shown at initial and final time for JANUARY-EXT and JULY. Both spectra show very little energy in the large scales at initial time and the JULY spectra also lack energy in the smaller scales from total wavenumber 35 onwards. At final time the JULY SV's remain smaller scale than the JANUARY SV's, with energy peaking around total wavenumber 13 and 9 respectively.

3.3 Geographical location

In Fig. 5a,b the root mean square (RMS) of streamfunction is displayed for JANUARY (default set) at initial and final time at level 22 (55 hPa). Initially, the S-SV's are mainly located over the Eurasian continent and east of Japan. The preferred location of the initial JANUARY S-SV's, corresponds closely with the location where the largest background horizontal zonal wind velocities and gradients occur. This can be seen when comparing Figures 5a and 6a. The latter figure shows the zonal background wind at 50 hPa, averaged over the 31 days of January 2004, 2005 and 2006.

The S-SV's east of Japan, are located lower (initially between 50–95 hPa) in the stratosphere than the S-SV's over Asia (initially between 15–55 hPa). This is due to the strong tropospheric jet that extends up to 70 hPa above of Japan, see Fig. 6b.

The initial JULY S-SV's are located (almost) everywhere within the 30° to 60°N latitude band, but they have a clear preference for certain locations, as can be inferred from Fig. 5c. At final time however, almost all amplitude is above the Eurasian continent at 40°N, see Fig. 5d. The JULY S-SV's are mostly located in the lower part of the vertical target zone (between 70 to 95 hPa).

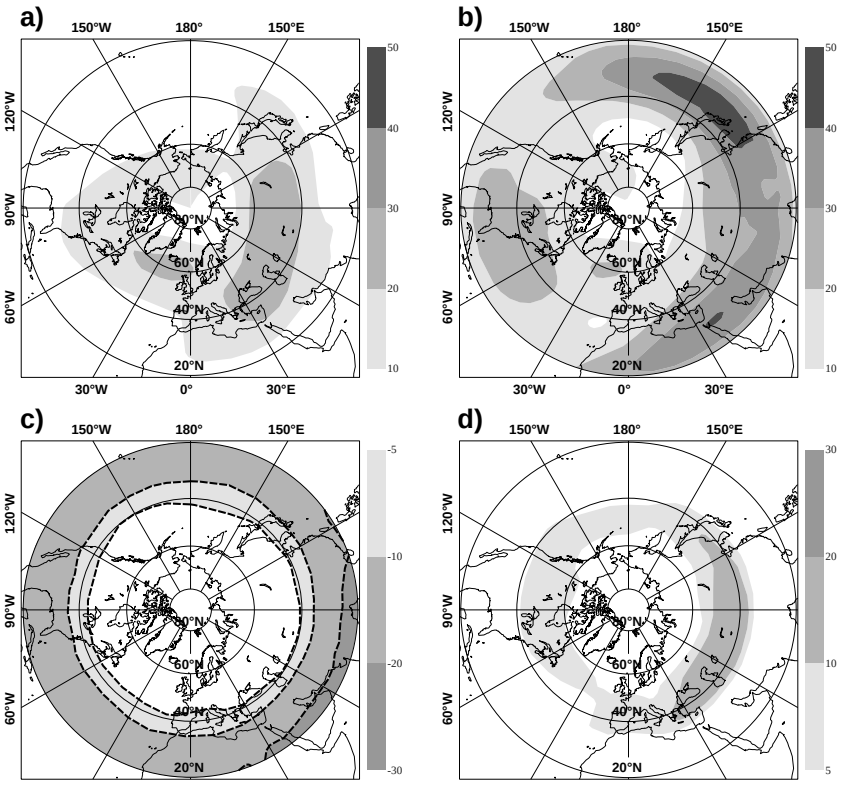

Figure 6: Monthly mean zonal background wind (ms^{-1}), north of 20°N, computed from daily data over the years 2004 to 2006, for (a) January at 50 hPa, (b) January at 100 hPa, (c) July at 50 hPa, and (d) July at 100 hPa. Negative values are denoted by a dashed contour line around the shaded area (only applicable for c). Pressure levels 50 and 100 hPa correspond (roughly) to model level 22 and 25, respectively.

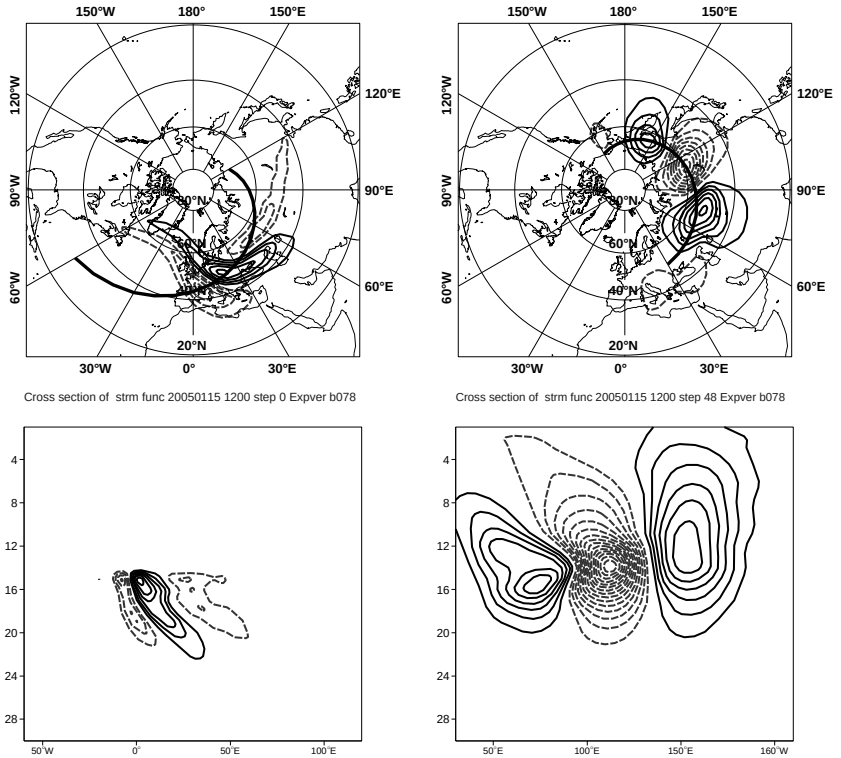

Figure 7: Streamfunction field for the leading S-SV of 15 January 2005 (a) at level 20 at initial time, (b) at level 18 at final time. (c) and (d) show the vertical cross-section of the S-SV's shown in a,b, respectively, over the model levels 1 to 30. The thick solid lines in a,b give the location of the vertical cross-section displayed in c,d. Contour interval used: in (a) 0.5, x, 10^4 m^2s^{-1} and 20 times larger for (b); in (c) 1.0, x 10^4 m^2s^{-1} and 20 times larger for (d).

Also for JULY, the preferred location of the S-SV's can largely be explained by analyzing the average zonal background wind during this month. In Fig. 6c the average July background zonal wind is shown at 50 hPa. The flow is almost completely zonal and so is characterized by extremely weak longitudinal gradients. Also the latitudinal gradients are weak. At 100 hPa (Fig. 6d), the flow is characterized by stronger gradients in the latitudinal and longitudinal direction (especially over Asia), as compared to 50 hPa. The strong preference of JULY S-SV's for the lower part of LS confirms once again, that the location of S-SV's is mostly where large background horizontal shears and velocities occur.

From Figs. 5a–d it is clear, that the January S-SV's propagate north-eastwards and that the propagation speed of July S-SV's is close to zero.

3.4 Examples of the S-SV's

In Fig. 7, a horizontal and vertical cross section of the leading S-SV of 15 January 2005 at initial and final time are shown. Initially (Fig. 7a), this S-SV is a twisted-distorted wavetrain that is tilted (Fig. 7c) against the shear of the background wind (the background wind above 50 hPa is eastwards and increases, due to the intensifying polar vortex, with height). During forecast time, the S-SV grows into a larger-scale wavetrain, see Fig. 7b (in accordance with Fig. 4). At final time there is hardly any vertical tilt left and the S-SV extends into the high stratosphere till the upper model level (Fig. 7d). This is an example of a JANUARY S-SV, as mentioned in section 3.2, that initially has its maximum energy around level 18 and during its amplification transmits energy into the HS.

An example of a JULY case is shown in Fig. 8. Both at initial and final time, this JULY S-SV consist of a clear wavetrain pattern (Fig. 8a,b). At initial time the S-SV is strongly tilted (Fig. 8c) against the shear of the background wind (the background wind above 100 hPa is westwards, but decreases fast with height and changes direction above 60 hPa, see Fig. 6c, d). At final time an almost equivalent barotropic pattern emerges (Fig. 8d). Instead of transmitting energy upwards, as in the former example, this S-SV propagates downwards to the troposphere.

3.5 S-SV's with a 5 day OTI

The average singular value of the mean of the 10 leading 5-day S-SV's is 6.7 and the standard deviation is 1.8. The values for the 2-day case are 4.0 and 0.4, respectively. So, extending the OTI results in stronger growth albeit less pronounced as it is in case of ST-SV's (see section 4.5).

The average growth of the TE with time over the vertical column for the 5-day S-SV's (not shown) shows the same relative growth over the 4 components as in the 2-days case (Fig.e 3a). Also for the 5-day case almost no energy is found in the LT.

The horizontal energy spectrum for the 5-day S-SV's (not shown), is nearly identical compared to the 2-day S-SV's (Fig. 4). The same applies for the location in terms of RMS of streamfunction for the 5-day ST-SV's compared with the 2-day ST-SV's.

Overall we conclude that, apart from the higher singular values, the 5-day S-SV's are very similar to 2-day S-SV's.

4 Stratosphere-Troposphere SV's

4.1 Amplification

Figure 9a displays the singular values of the leading ST-SV's and the mean singular value of the ten leading ST-SV's of JANUARY-EXT. The leading singular values have an average value of 0.86 and a maximum value of nearly 1.4. The values for JULY as presented in Fig. 9b are smaller than for JANUARY-EXT, with no values exceeding one. The leading singular JULY values are on average 0.74, with a maximum value close to 1. In Fig. 9c the averaged singular values as a function of the index number is shown. For JANUARY-EXT and JULY the lines have identical slopes.

Although most of the ST-SV's have singular values smaller than one, this does not necessarily mean that ST-SV's are decaying (below 500 hPa). From Fig. 10, discussed in the next section, it is immediately clear that the ST-SV's remain growing in the LT after optimization time. In fact, ST-SV's with an OTI of 5 days yield singular values considerably larger than one (see section 4.5).

4.2 Energy distribution

In Fig. 10a, it is shown how the leading ST-SV's of JANUARY-EXT grow with time over the vertical column in terms of TE. Similar to section 3.2 the vertical column is partitioned into four parts. At initial time unit TE is in the LS. The TE below 500 hPa (dashed-dotted) is zero at t=0 and becomes almost 1 at optimization time. To show that for larger OTI's we do achieve amplification in the LT, the same result obtained for an OTI of 5 days is shown in Fig. 10b. Clearly, the larger OTI results in amplifying ST-SV's, which grow in the TE norm by a factor larger than 40, corresponding to singular values above 6. The different projection operator used at final time (as compared with the S-SV's) has resulted in SV's that are capable of producing significant perturbation growth in the LT. The amount of perturbation energy in the HS at final time is negligible. Notice that the perturbation energy growth in the LS for the 2-day case, levels off between 24 and 36 hours. For the 5-day case

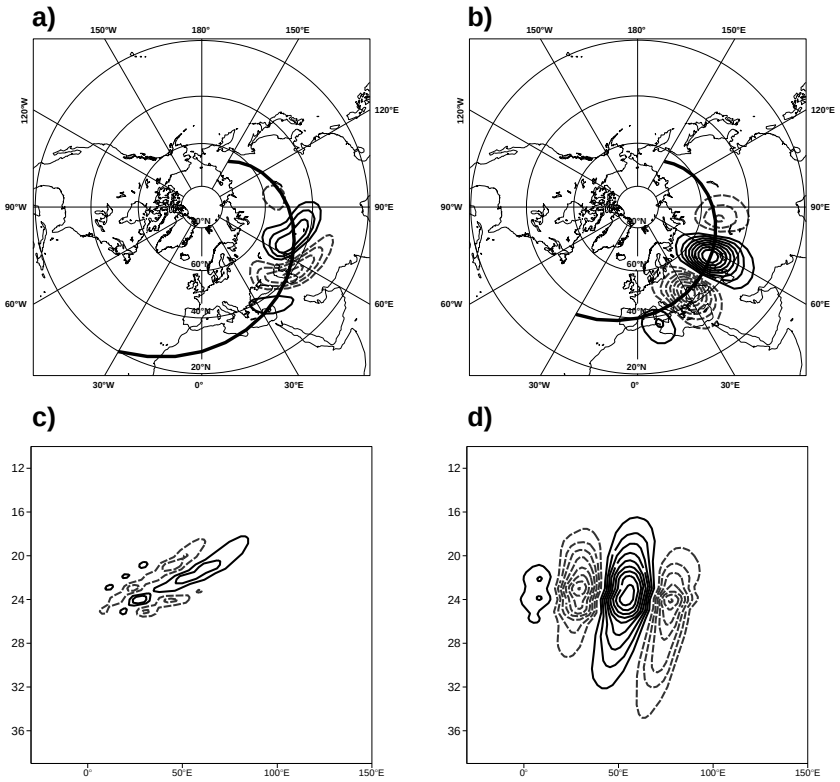

Figure 8: (a–d) As in Fig. 8 but for the leading S-SV of 8 July 2005. In b the horizontal cross-section is now taken over level 20. In c,d the vertical cross-sections are now taken over the model levels 11 to 40. Contour interval used: in (a) 0.5 x $10^4 m^2 s^{-1}$ and 4 times larger for (b); in (c) 1.0 x $10^4 m^2 s^{-1}$ and 4 times larger for (d).

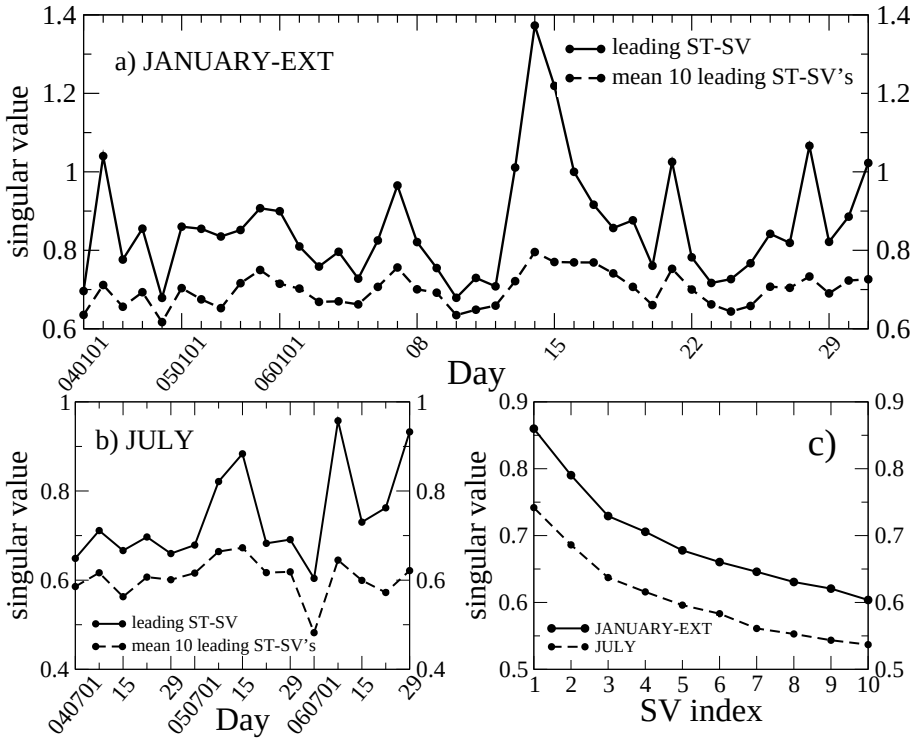

Figure 9: The leading singular value (solid line) and the mean singular value of the ten leading ST-SV's (dashed line) of (a) JANUARY-EXT, and (b) JULY. (c) Averaged singular value of the ten leading ST-SV's as a function of their index, for JANUARY-EXT (solid) and JULY (dashed).

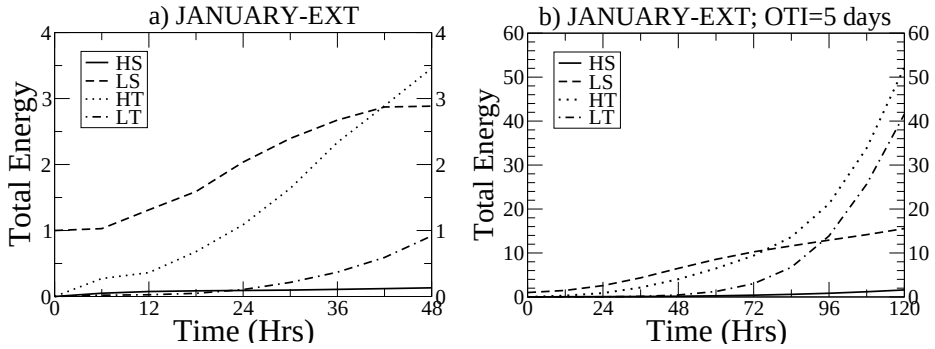

Figure 10: As Fig. 3 but for the leading ST-SV's of (a) JANUARY-EXT, and (b) JANUARY-EXT with an OTI of 5-days.

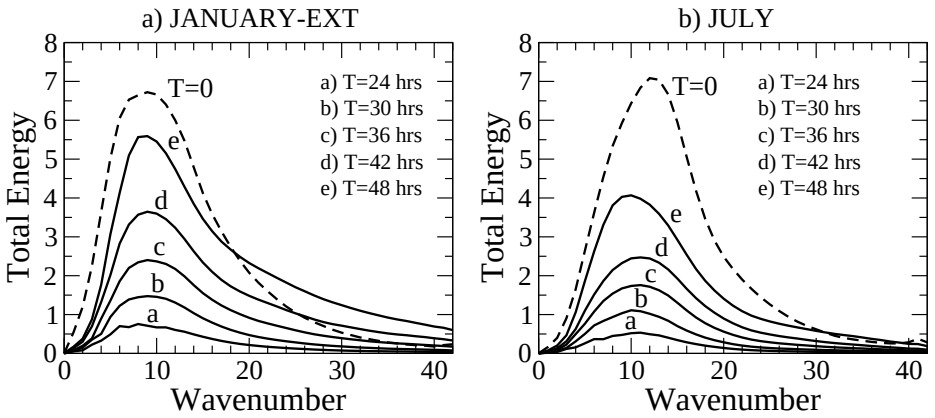

Figure 11: Total wavenumber spectra for the leading ST-SV's of (a) JANUARY-EXT, and (b) JULY are shown for different forecast times and restricted to the lower troposphere (below 500 hPa). The dashed line shows the initial time spectra. Values are multiplied by a factor 100.

this is less clear, but also here perturbation growth decreases after 72 hours.

The ST-SV's calculated with an OTI of 5 days are further discussed in section 4.5. Here and in the following 2 paragraphs the 2-day ST-SV's are discussed.

In Fig. 11a, b, the average time evolution of the horizontal spectra, restricted to the TE in the LT, are shown for the leading ST-SV's of JANUARY-EXT and JULY, respectively. The initial time spectra, when the SV's are confined to the LS, are given as well. Broadly speaking the behavior in JANUARY and JULY are similar and both the initial time ST-SV's (in the LS) and the structures developing in the LT are dominated by total wavenumber 9–10. The perturbation growth in the LT seems to lack the up-scale perturbation growth present in the growth mechanism of tropospheric SV's, and to a lesser extend of S-SV's (see Fig. 4).

The KE part of the ST-SV's (both for January and July) at initial time is larger than it is for S-SV's and amounts on average to 65 % of the total. At final time this has, on average, increased to 78 % (not shown).

4.3 Geographical location

In January the ST-SV's seem to favor exactly those areas where baroclinic instability is maximal in the troposphere (Fig. A3a in appendix A.2). The initial time RMS of streamfunction field at level 22 (Fig. 12a), shows two centers of activity: the West Pacific and the Western Atlantic. These are also the areas where perturbation growth occurs at final time at 500 hPa, as shown in Fig. 12b. Also for JULY (Fig. 12c, d), ST-SV's are located, where baroclinic instability is high in the troposphere (Fig. A3b, appendix A.2): above Asia and Canada.

4.4 Example of the ST-SV's

Figure 13 shows the perturbation streamfunction of a typical JANUARY (13a,b) and JULY (13c,d) ST-SV at initial time in the LS and at final time for the level where it enters the LT. Both leading ST-SV's reveal well defined wavetrains, with more poleward located structures at final time.

The initial ST-SV's are strongly tilted eastward with height for both JANUARY and JULY. In January the average background wind between 100 and 50 hPa is eastward and decreases with height (due to the weakening of the tropospheric jet. In July the average background wind above 100 hPa is eastward, but decreases fast with height and becomes westward above 60 hPa. During the forecast, untilting of the initial time structure takes place and the perturbation extracts energy from the background flow (see HOSKINS et al., 2000).

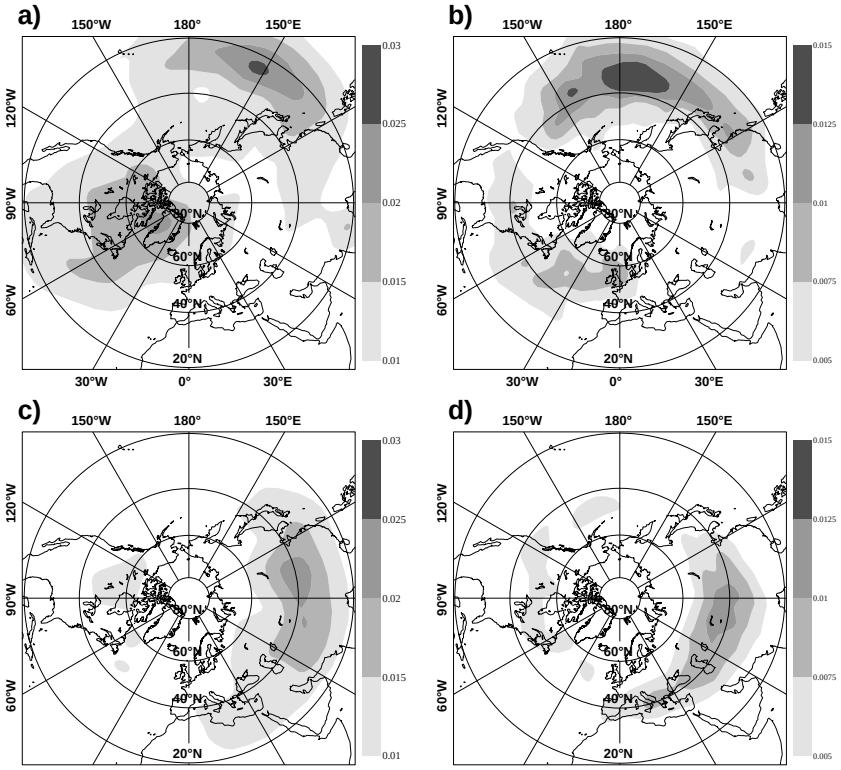

Figure 12: RMS of streamfunction (m^2s^{-1}) of the 10 leading ST-SV's of (a) JANUARY at level 22 at initial time, (b) JANUARY at level 39 at final time, (c) JULY at level 22 at initial time (d) JULY at level 39 at final time. Values have to be multiplied with 1.0 x $10^6 m^2 s^{-1}$. Notice that the values at final time are a factor 2 smaller than at initial time.

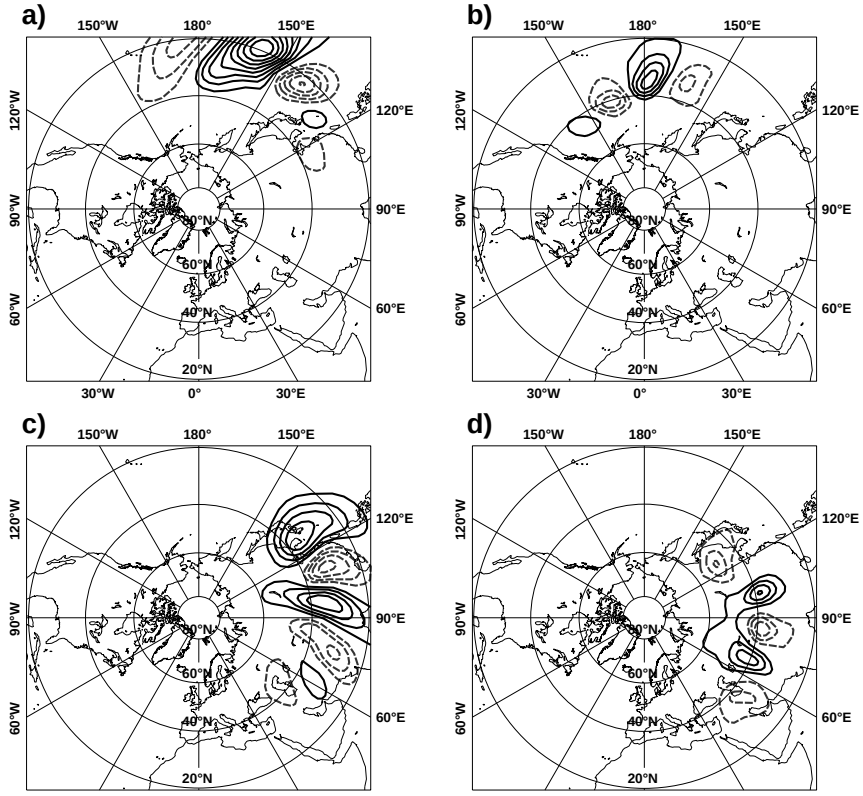

Figure 13: Streamfunction field of the leading ST-SV of 8 January 2006 (a) at initial time at level 22, (b) at final time at level 39, and of the leading ST-SV of 29 July 2004 (c) at initial time at level 22, (d) at final time at level 39. Contour interval in (a,b,c) is 1.0 x 10^4 $m^2 s^{-1}$ and in (d) is half this value. Dashed (solid) lines denote negative (positive) values.

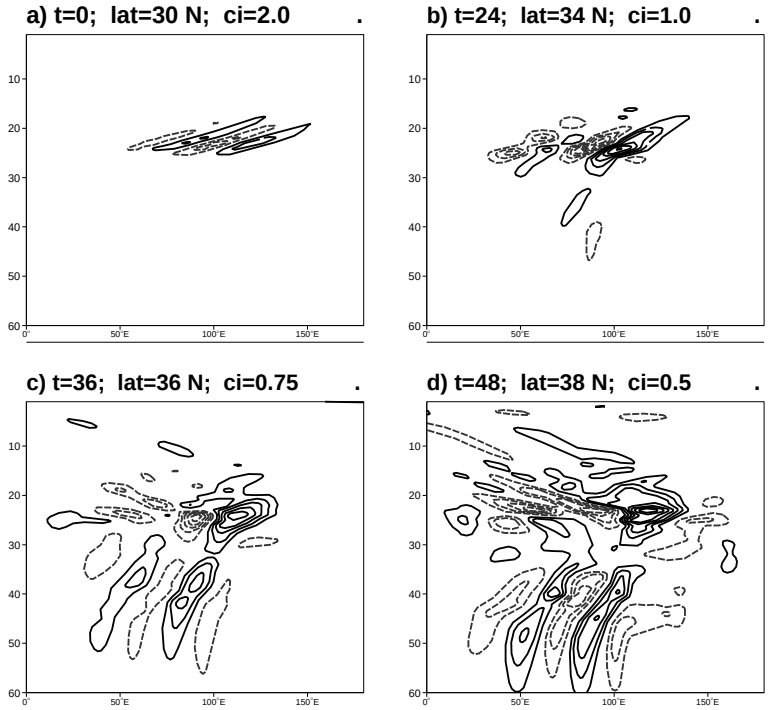

Figure 14: Time evolution of the cross-section of the leading ST-SV in terms of streamfunction (m^2s^{-1}), from 1200 UTC 29 July 2004 for t=0, t=24, t=36 and t=48 hours. Above each panel forecast time and contour interval (ci) is given; values have to be multiplied with 1.0 x 10^4 m^2s^{-1}. Dashed (solid) lines denote negative (positive) values. The latitude, where the cross-section is taken, is shifted by 1 degree north every 6 hours, to compensate for the poleward movement of the SV during the forecast.

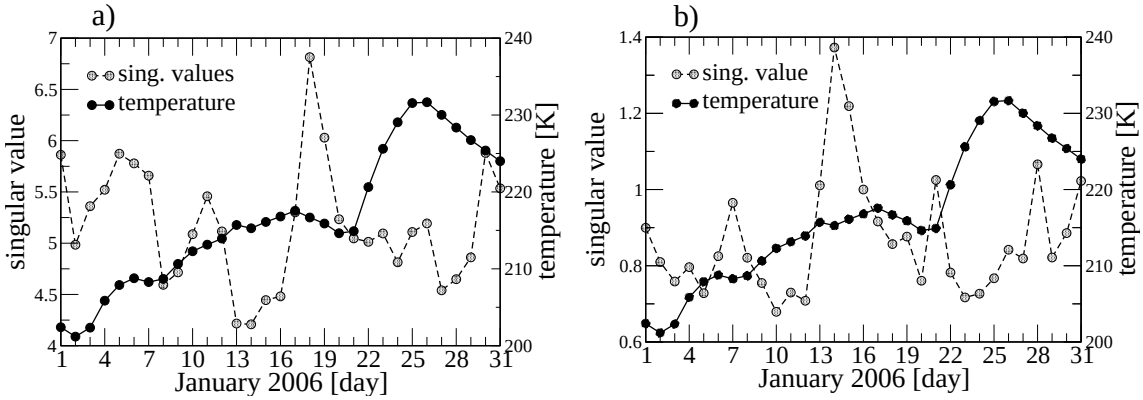

Figure 15: Leading singular values (dashed line) of (a) S-SV's, and (b) ST-SV's, calculated with an OTI of 2 days are displayed for January 2006. Also shown in the graphs, is the average temperature, north of $70^\circ N$, at 20 hPa (solid line).

To get a better understanding of the time evolution of such ST-SV's, we have plotted the vertical cross-section of streamfunction for a JULY case for four chosen forecast times (Fig. 14). Initially this is a strongly eastward tilted structure. At t=24 hrs part of the perturbation has reached the LT, where it amplifies during the remainder of the forecast. Notice that the eastward tilt in the LS has changed in the final 24 hrs of the computation from an eastward to a westward tilted structure.

4.5 ST-SV's with a 5-day OTI

To investigate whether large further amplification is possible with ST-SV's, we have also calculated ST-SV's with an OTI of 5 days.

The average singular value of the mean of the 10 leading 5-day ST-SV's is 3.1 with a standard deviation of 0.5 (not shown). This should be compared with the values of the 2-day ST-SV's (Fig. 9a), which are respectively 0.7 and 0.04. So, extending the OTI, results in stronger amplification, as could already be anticipated from Fig. 10a.

Looking at the energy distribution over the 4 components for the 5-day case, as shown in Fig. 10b, we conclude that a 2-day forecast is just too short to produce amplifying SV's going from the LS to the LT. Notice further, that for the 5-day case, the perturbation TE in the LT exceeds the amount of perturbation TE in the LS, after approximately 4 days.

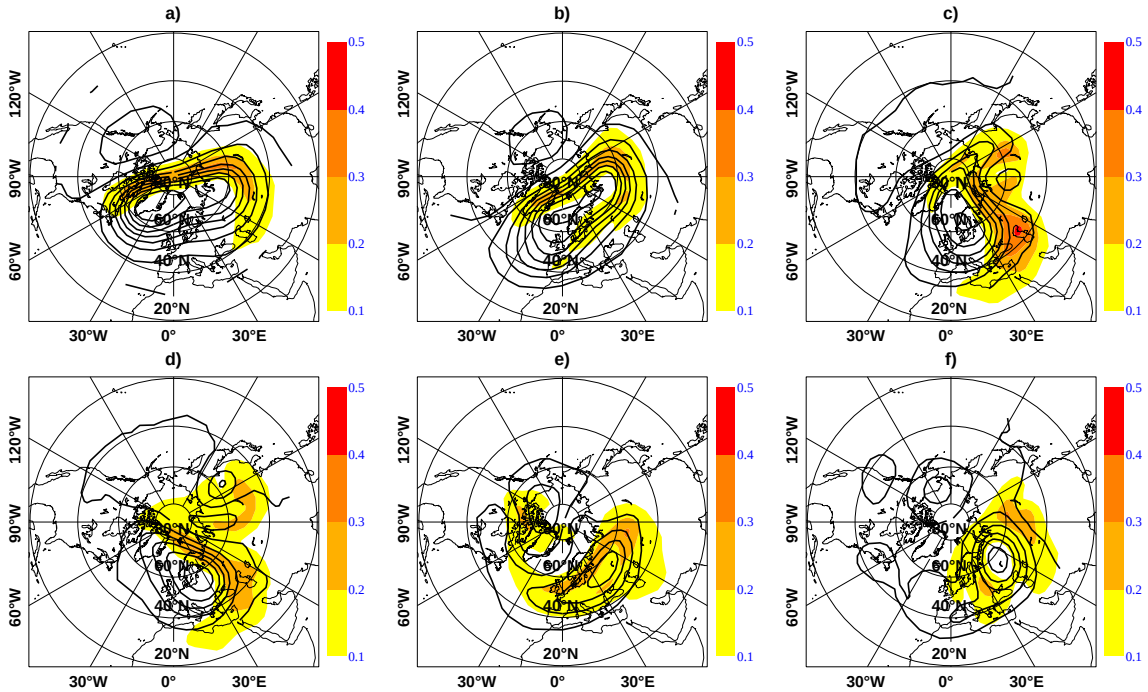

Figure 16: Background geopotential height field at 20 hPa (solid lines) together with the RMS of streamfunction (m^2s^{-1}) of the 10 leading, final time, S-SV's at model level 18 (∼23 hPa), for (a) 13 (b) 17 (c) 21 (d) 23 (e) 27 and (f) 31 of January 2006. The final time S-SV's are evolved (OT=48 h) from the initial time S-SV's that started 2 days before the dates of (a–f). Contour interval of the geopotential height is 200 *m* and the RMS values have to be multiplied with 1.0 x 10^6 m^2s^{-1}.

The horizontal energy spectrum for the 5-day ST-SV's (not shown) is almost identical to the 2-day case (Fig. 11a).

The preferred locations of the 5-day ST-SV's (not shown) are very similar to the 2-day case. One difference is noticed: for the 5-day case the two preferred locations in January (the West Pacific and the Atlantic Ocean as found for the 2-day ST-SV's, Fig. 12b) are at final time more clearly connected, due to a strip of high(er) amplitude over the East Pacific and the USA.

Overall, we can conclude that 5-day ST-SV's are very similar to the 2-day ST-SV's.

5 Connection with tropospheric SV's

In section 4.3 we mentioned that at final time the ST-SV's are located at those areas where baroclinic instability processes are likely to occur. These are the areas where in general also tropospheric SV's (T-SVs) are found (BUIZZA and PALMER, 1995). For this reason, it is plausible that the ST-SV's, in the troposphere, make use of the same perturbation growth mechanisms as T-SV's do, and therefor that the ST-SV's project for a certain forecast time on the T-SV's. In order to quantify to what extent ST-SV's project on the T-SV's,we make use of the similarity index (BUIZZA, 1998). This index measures how similar subspaces are spanned by the leading SV's, and ranges from 0 (orthogonal) to 1 (identical).

From Fig. 10a we noticed that (for an OTI of 2 days) the energy in the LT starts to grow rapidly only after 24 hours. The first 24 hours are presumably needed to get a small but significant amount of perturbation energy in the LT and HT. Subsequently, this perturbation energy is (strongly) amplified by baroclinic instability processes. We have verified this hypothesis by calculating the similarity of ST-SV's with two types of T-SV's. T-SV's are calculated:

i) from the same time and date as the JANUARY and JULY sets and with the same OTI of 48 hours (T-SVs_00).

ii) from the forecast 24 hours after the initial dates of the JANUARY and JULY sets, and with an OTI of 24 hours (T-SVs_24).

In both the cases the T-SV's are optimized to maximize the growth of TE below level 25 (96 hPa).

The similarity index is calculated between the spaces spanned by the ten leading ST-SV's and ten leading T-SVs (for both the types), at final time and below 500 hPa.

The similarity between the ST-SV's and T-SVs_00, ranges for JANUARY between the 8 and 28 %, and so the subspaces are quite uncorrelated. The similarity is even much lower with the T-SVs_24, all values are below 10 %. For July the similarity of the ST-SV's with the T-SVs_00 is between 0 and 30 % and with the T-SVs_24 again lower, mainly all values are below 10 %.

So, opposite to what we expected, the ST-SV's are clearly more highly correlated with tropospheric SV's

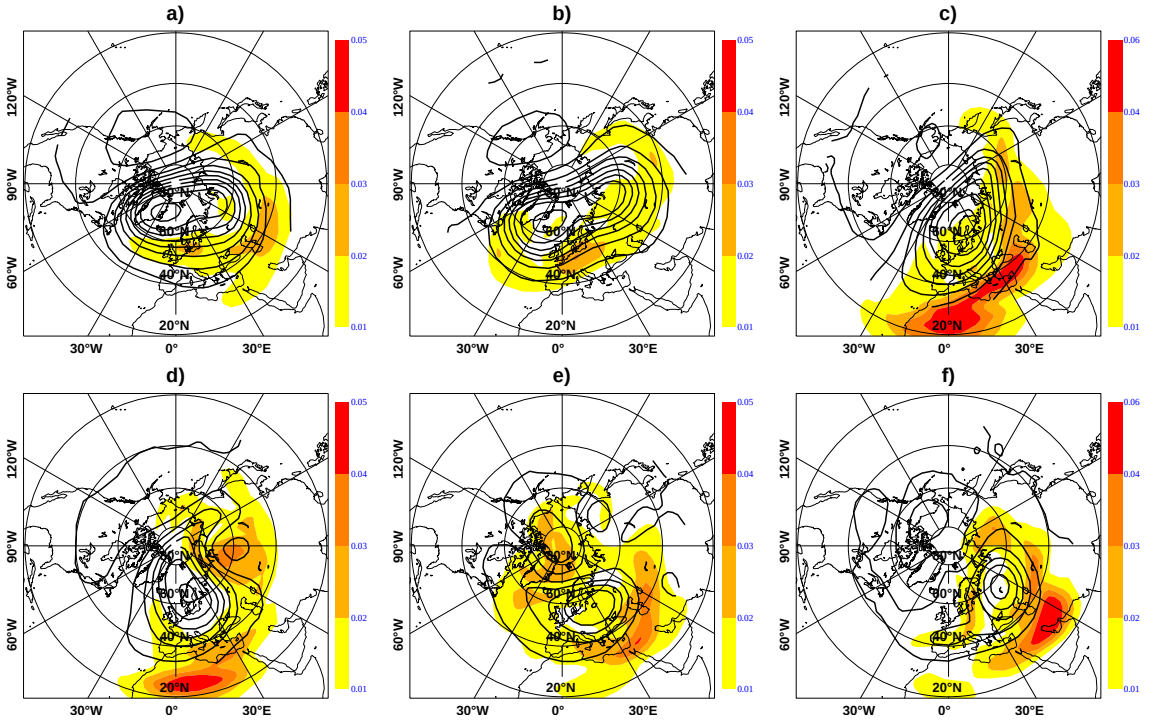

Figure 17: As Fig. 16 but for the initial time S-SV's as mentioned below Fig. 15 for the days (a) 11 (b) 15 (c) 19 (d) 21 (e) 25 and (f) 29 of January 2006, with corresponding background geopotential height field at 20 hPa. Contour interval of the geopotential height is 200 *m* and the RMS values have to be multiplied with 1.0 x 10^6

which start at the same date and time, than with tropospheric SV's calculated from the forecast 24 hours later.

We have also calculated the similarity of the (10 leading) ST-SV's with the (10 leading) S-SV's. The JANUARY ST-SV's are mainly located over different areas compared with the corresponding set of S-SV's (compare figures 5b and 12b). Further, for JANUARY the majority of S-SV's are located higher in the stratosphere than the ST-SV's. In fact, only the S-SV's east of Japan, which are located lower in the stratosphere than the majority of S-SV's (see section 3.2), can significantly contribute to the similarity with the ST-SV's. This results in an average similarity between the 2 sets (at final time and between the levels 15 to 25) below 10 %. Individual similarities between the S-SV's located east of Japan with some of the ST-SV's, give values up to 70 %. For July the ST-SV's and S-SV's are located over more similar areas, and also at similar heights. The similarity, again at final time and from level 15 to 25, is however still low, on average 20 %.

6 Stratospheric sudden warming January 2006

As mentioned at the end of section 2, a major SSW event occurred from the 21th of January 2006.

From the 3rd of January (see solid line in Fig. 15a) the temperature started to rise and the warming was identified as a minor event. From the 21th of January the temperature increased even further, the vortex split, and above 30 hPa, the meridional gradient of temperature reversed making the event a major warming event (CHARLTON and POLVANI, 2007)

It is of interest whether the occurrence of the SSW is reflected in the basic properties of the S-SV's and ST-SV's, such as their singular values and their preferred geographical location.

In Fig. 15a,b the leading singular values of the S-SV's and ST-SV's calculated with an OTI of 2 days are shown, together with the average temperature north of 70°N, at 20 hPa. From these figures we conclude that the occurrence of the SSW is not reflected in the singular values of either the S-SV's or ST-SV's. The singular values of the S-SV's and ST-SV's calculated with an OTI of 5 days, show a mainly similar behavior over this month as their 2-day counterparts and so, they (also) do not correlate with the average temperature at 20 hPa.

To study if the preferred location of the S-SV's changes during the SSW event, we show in Fig. 16 the RMS of streamfunction of the 10 leading final time S-SV's for 6 days between 13 to 31 January 2006, together with the corresponding background geopotential height fields at 20 hPa. We have chosen the 20 hPa level, because at this height the split of the polar vortex is a dominant feature, and it coincides with the level where the S-SV's achieve their maximal amplitude in TE (see also Fig. A2a in appendix A.1).

From these plots we conclude that the evolved S-SV's are located where the highest velocity shears occur. The RMS pattern closely resembles the shape of the polar vortex, as is clearly visible in Fig. 16a–f. Also the RMS area breaks up in two distinct areas (Fig. c–e), at the same time when the polar vortex does.

Figure 17 is similar to Fig. 16, but now the RMS of the initial time S-SV's, associated with the evolved S-SV's of Fig. 16, are shown together with the corresponding background geopotential height fields at 20 hPa. The S-SV's have, at initial time, significant amplitude outside the polar vortex. So, we observe that S-SV's tend to propagate from the outer edges of the vortex into the strong jet, where they end up at locations with large horizontal shears (see also HARTMANN et al., 1996).

7 Conclusions

A recent version of the ECMWF model that extends well into the high stratosphere (up to 0.1 hPa), has been used to calculate stratospheric SV's (S-SV's) that are uptimized to amplify between 96 and 12 hPa for an optimization time intervall (OTI) of 2 days.

These S-SV's amplify more than 25 (7) times in terms of TE in January (July) during two days. The preferred total wavenumber for the perturbation structures at initial time is around wavenumber 18 for both January and July, and shifts to larger scales, wavenumber 9 and 13, respectively, at final time. The preferred location of the S-SV's is where the background zonal velocity gradients are large. This leads to two types of S-SV's in winter: the majority of S-SV's amplify due to the polar vortex. The remainder of the S-SV's are located lower, around 80 hPa and amplify on the Pacific tropospheric jet, which may extend above 100 hPa. The S-SV's found for July, are similar in form, structure and amplification mechanism as the latter type of winter S-SV's.

Further 5-day OTI S-SV's have been calculated. The amplification in TE norm is a factor of 3 larger than for their 2-day counterparts. All other basic properties are quite similar.

To study whether the occurrence of a SSW is reflected in the S-SV properties, we have calculated S-SV's during the SSW of January 2006. The amplification factor of the S-SV's does not seem to be affected by the SSW. The breaking of the polar vortex is however clearly reflected in the preferred geographical location of the S-SV's. The prefered location of the evolved S-SV's follows very clearly the locations of highest horizontal velocity gradients and it splits in two distinct areas at the same moment as the polar vortex breaks up. During the SSW, stratospheric structures mainly amplify by propagating from the outer edges of the polar vortex into the polar vortex (as was also reported by HARTMANN et al., 1996). We intend to substantiate these results by considering more SSW occurrences. Further we will study to what extent stratospheric and upward propagating (tropospheric-stratospheric) SV's are capable of triggering SSW's or prevent them from happening.

We have made a preliminary study of the possible role of linear non-modal perturbation growth in the stratosphere-troposphere interaction. For this reason we have calculated perturbations that are optimized to cross the tropopause and to enter in the lower troposphere (below 500 hPa). Allowing only an OTI of 2 days for this process proved to be too short to produce amplifying structures. However, by increasing the OTI to 5 days, we found amplifying ST-SV's with singular values exceeding 6. The basic properties of the ST-SV's with a 2 or 5 day OTI are very similar.

The ST-SV's produce perturbation growth in the stratosphere albeit with smaller amplitude than the S-SV's. It appears that ST-SV's quickly transfer perturbation energy to tropospheric regions, where baroclinic instabilities are likely to occur. Given the amplification factors of ST-SV's and the fact that they are more subject to linear dynamics than there tropospheric counterparts (e.g. JUNG and BARKMEIJER, 2005), one may envisage a role of ST-SV's in future ensemble prediction systems.

We have verified that evolved ST-SV's resemble more evolved tropospheric SV's calculated for the same forecast and OTI, than evolved tropospheric SV's calculated for the atmosphere 24 hours later and with an OTI of 1 day.

Acknowledgments

This research is supported by the Research Council for Earth and Life Sciences (ALW) of the Netherlands Organization for Scientific Research (NWO). The authors would like to thank W.T.M. VERKLEY and four anonymous referees for helpful comments and suggestions.

Appendix

A.1 Choice of initial projection operator

Calculating ST-SV's with an initial projection operator that includes all model levels above level 26 (P_{ini}^{1-25}), results for the majority of the cases in ST-SV's with a vertical TE distribution similar to the one displayed in Figure A1a.

To avoid difficulties with spurious growth near the top level, which occurred in some cases, we decided to employ an initial projection operator between the levels 15 and 25. In fig. A1b, the vertical energy distribution for the leading ST-SV of the same day as in Fig. A1a, but now calculated with P_{ini}^{15-25} (including level 15 to 25), is shown. The shape of the distribution is the same as in A1a. The similarity index between the subspaces spanned by the 10 leading ST-SV's computed by using respectively: the P_{ini}^{1-25} and the P_{ini}^{15-25} projection

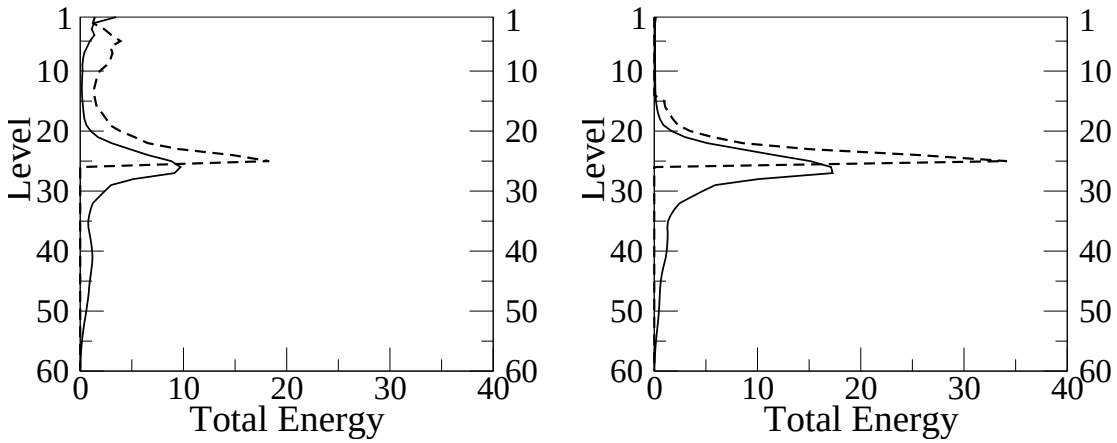

Fig A1: Vertical distribution of the total energy for the leading ST-SV of the 1st of January 2004 as a function of model level. Computed with an initial projection operator that includes (a) levels 1–25, and (b) levels 15–25. The initial (final) time distribution is displayed by the dashed (solid) line. Final time energy is multiplied by a factor 0.2.

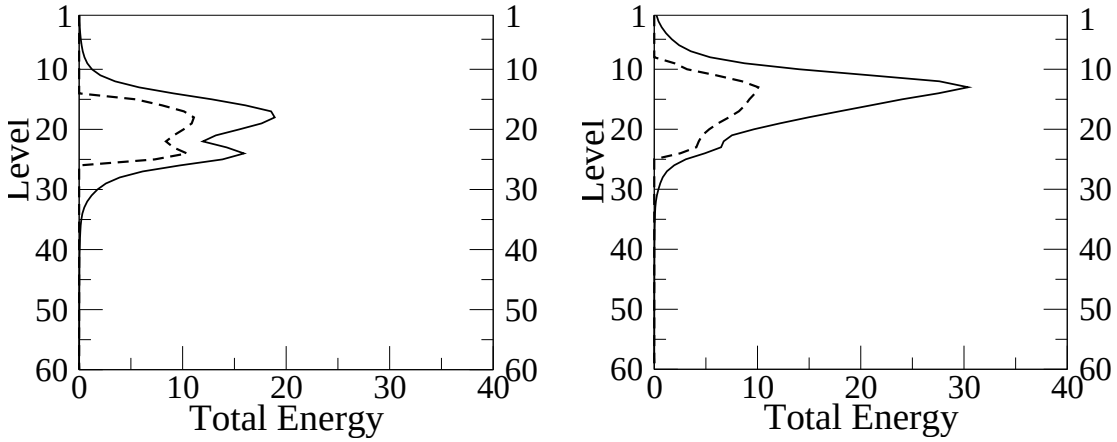

Fig A2: Vertical distribution of the mean total energy for the 10 leading S-SV's of JANUARY (default set), as a function of model level. Computed with an initial and final time projection operator that includes (a) levels 15–25, and (b) levels 10–25. The initial (final) time distribution is displayed by the dashed (solid) line. Final time energy is multiplied by a factor 0.1.

operator, has been calculated for 5 days in January and 5 days in July 2004. The similarity index between the two sets, at initial time and between the levels 15 to 25, is 85 % for January and 75 % for July. At final time and calculated below 500 hPa (the P_{evo} region), the similarity is 80 % for January and 70 % for July. These high similarities show, that excluding the upper 14 model levels results in quite similar initial and final time structures.

The lower boundary of the projection area ensures that an important portion of the stratosphere dynamics is captured while keeping initial time structures away from the tropopause height. To see what the effect on the ST-SV's is, when the lower boundary of the initial projection operator is lowered by one level, we have done additional ST-SV calculations with an initial projection operator (P_{ini}^{15-26}) that also included level 26 (113 hPa). The average similarity index between the subspaces spanned by the 10 leading ST-SV's computed respectively by the use of the P_{ini}^{15-25} and the P_{ini}^{15-26}, is at initial time 83 % (over the levels 15 to 25) and at final time 77 % (over the level 39 to 60), and indicate that the SV's resulting from both computations are quite similar.

We also verified whether the results for the S-SV's would become significantly different, when the upper boundary of the P_{ini} (=P_{evo}) projection operators is increased with 5 levels. In fig. A2 the average vertical TE distribution for the JANUARY (default) S-SV set is shown for two cases. In (a) S-SV's are calculated with the (default) $P_{ini,evo}^{15-25}$ and in (b) with $P_{ini,evo}^{10-25}$. Although more S-SV's are located higher in the atmosphere for the $P_{ini,evo}^{10-25}$ case, where they grow on the polar vortex, the similarity between the two sets (between level 15 to 25) is very high and amount to 80 % at initial and final time.

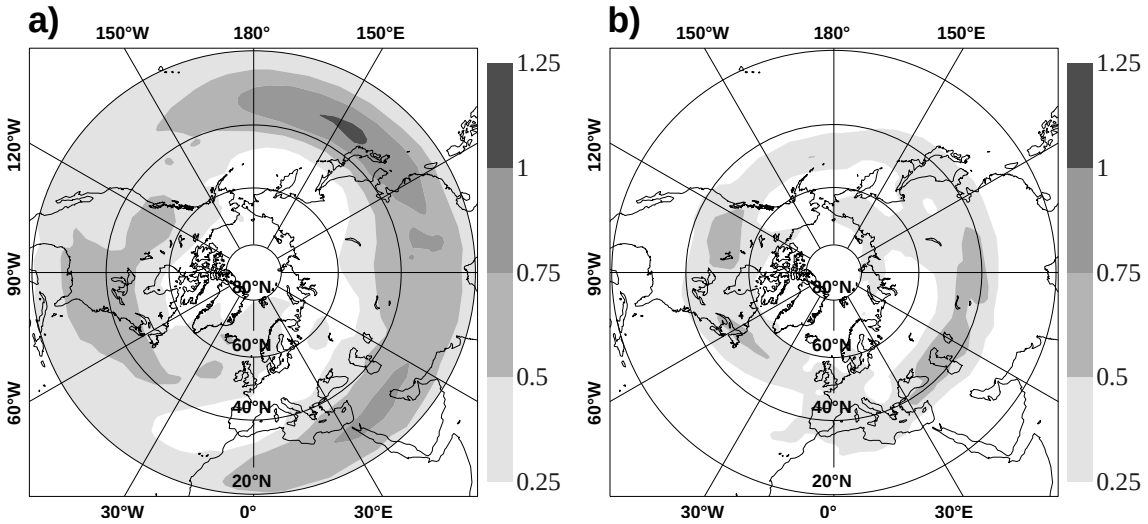

Fig A3: Distribution of the Eady index in the troposphere (a) January, and (b) July. Based on the climatological mean of averaged daily data of January and July 2004–2006, calculated between 250 and 1000 hPa.

A.2 Eady index

To quantify where baroclinic instability is likely to occur in the troposphere, we have calculated the Eady index between 250 and 1000 hPa. The Eady index (e.g. see HOSKINS and VALDES, 1990) is defined as:

$$\sigma_E = 0.31 \frac{f}{N} \frac{du}{dz} \qquad (7.1)$$

with f the Coriolis parameter. To get an estimate for the static stability of the atmosphere (N, see e.g. HOLTON, 2004) and the vertical wind shear (du/dz), we have made use of the climatological mean (computed from daily data over the months January and July for the years 2004–2006 from the ECMWF archives) of the potential temperature and the zonal wind. In Fig. A3 the result is shown for (a) January, and (b) July. In section 4.3 it is noted that the preferred locations of the ST-SV's coincide with the areas that are characterized by a high Eady index: the West Pacific and the Western Atlantic. The ST-SV's are not located above North Africa, which area is also dominated by a high Eady index. The region above North Africa is however not known as a region with strong instability, in so far as it is not associated with high climatological transient variability. So it seems, that the ST-SV's correctly exclude this region as an area of high instability. Interestingly enough, tropospheric SV's do pick (erroneously) this region as a region of high instability (see further, BUIZZA and PALMER, 1995).

References

ANDREWS, D.G., J.R. HOLTON, C.B. LEOVY, 1987: Middle atmospheric dynamics. – Acadamic Press. 489 pp.

BALDWIN, M. P., J. DUNKERTON, 1999: Propagation of the Arctic Oscillation from the stratosphere to the troposphere. – J. Geophys. Res. **104**, 30937–30946.

BALDWIN, M.P., D.B. STEPHENSON, D.W.J. THOMPSON, T.J. DUNKERTON, A.J. CHARLTON, A. O'NEILL, 2003: Stratospheric memory and skill of extended-range weather forecasts. – Science **301**, 636–640.

BOVILLE, B.A., 1984: The influence of the polar night jet on the tropospheric circulation in a GCM. –Science **41**, 1132-1142.

BUIZZA, R. 1998:Impact of horizontal diffusion on T21, T42, and T63 singular vectors. – J. Atmos. Sci. **55**, 1069–1083.

BUIZZA, R., T.N. PALMER, 1995: The singular vector structure of the atmospheric global circulation. – J. Atmos. Sci. **52**, 1434–1456.

CHARLTON, A.J., L.M. POLVANI, 2007: A new look at stratospheric sudden warmings. Part I: climatology and modeling benchmarks. – J. Climate **20**, 449–469.

CHARLTON, A.J., A. O'NEILL, D.B. STEPHANSON, W.A. LAHOZ, M.P. BALDWIN, 2003: Can knowledge of the state of the stratosphere be used to improve statistical forecasts of the troposphere. – Quart. J. Roy. Meteor. Soc. **129**, 3205–3224.

CHRISTIANSEN, B., 2005: Downward propagation and statistical forecast of the near-surface weather. – J. Geophys. Res. **110**, D14104

ERRICO, R.M., 2000: Interpretations of the total energy and rotational energy applied to determination of singular vectors. – Quart. J. Roy. Meteor. Soc. **126A**, 1581–1599.

FARRELL, B.F., P.J. IOANNOU, 1996: Generalized stability theory. Part II: Nonautonomous systems. – J. Atmos. Sci. **53**, 2042–2053.

HARTMANN, D. L., T.N. PALMER, R. BUIZZA, 1996: Finite-time instabilities of lower-stratospheric flow. – J. Atmos. Sci. **53**, 2130–2143.

HAYNES, P, 2005: Stratosphere dynamics. – Ann. Rev. Fluid. Mech. **37**, 263–293.

HOLTON, J.R., 2004: An introduction to dynamic meteorology. – Elsevier Academic Press. 535 pp

HOSKINS, B.J., P.J. VALDES, 1990: On the existence of stormtracks. – J. Atmos. Sci. **42**, 1854–1864

HOSKINS, B.J., R. BUIZZA, J. BADGER, 2000: The nature of singular vector growth and structure. – Quart. J. Roy. Meteor. Soc. **126**, 1565–1580

JUNG, T., 2005: Systemetic errors of the atmospheric circulation in the ECMWF forecasting system. – Quart. J. Roy. Meteor. Soc. **131**, 1045–1073

JUNG, T., BARKMEIJER, J., 2005: Sensitivity of the tropospheric circulation to changes in the strength of the stratospheric polar vortex. – Month. Wea. Rev. **134**, 2191–2207.

KALNAY, E, 2003: Atmospheric modeling, data assimilation and predictability. – Cambridge University Press, 341 pp

KALNAY, E., KALNAY, E., M. KANAMITSU, R. KISTLER, W. COLLINS, D. DEAVEN, L. GANDIN, M. IREDELL, S. SAHA, G. WHITE, J. WOOLLEN, Y. ZHU, M. CHELLIAH, W. EBISUZAKI, W. HIGGINS, J. JANOWIAK, K.C. MO, C. ROPELEWSKI, J. WANG, A. LEETMAA, R. REYNOLDS, R. JENNE, D. JOSEPH, 1996: The NCEP/NCAR 40-Year Reanalysis Project. – Bull. Amer. Meteor. Soc. **77**, 437–471

O'NEILL, 2003: Stratospheric sudden warmings. – In: Encyclopedia of Atmospheric Sciences. J.R. HOLTON, J.A. PYLE, J.A. CURRY (Eds.), Elsevier, 1342–1353.

RANDEL, W., P. UDELHOFEN, E. FLEMING, M. GELLER, M. GELMAN, K. HAMILTON, D. KAROLY, D. ORTLAND, S. PAWSON, R. SWINBANK, F. WU, M. BALDWIN, M.-L. CHANIN, P. KECKHUT, K. LABITZKE, E. REMSBERG, A. SIMMONS, D. WU, 2004: The SPARC Intercomparison of Middle-Atmosphere Climatologies. – J. Climate **17**, 986–1003.

SONG, Y., W.A. ROBINSON 2004: Dynamical Mechanisms for Stratospheric Influences on the Troposphere. – J. Atmos. Sci. **61**, 1711–1725.

UPPALA, S.M., UPPALA, S. M., P. W. KÅLLBERG, A. J. SIMMONS, U. ANDRAE, V. DA COSTA BECHTOLD, M. FIORINO, J. K. GIBSON, J. HASELER, A. HERNANDEZ, G. A. KELLY, X. LI, K. ONOGI, S. SAARINEN, N. SOKKA, R. P. ALLAN, E. ANDERSSON, K. ARPE, M. A. BALMASEDA, A. C. M. BELJAARS, L. VAN DE BERG, J. BIDLOT, N. BORMANN, S. CAIRES, A. DETHOF, M. DRAGOSAVAC, M. FISHER, M. FUENTES, S. HAGEMANN, E. HÓLM, B. J. HOSKINS, L. ISAKSEN, P. A. E. M. JANSSEN, A. P. MCNALLY, J.-F. MAHFOUF, R. JENNE, J.-J. MORCRETTE, N. A. RAYNER, R. W. SAUNDERS, P. SIMON, A. STERL, K. E. TRENBERTH, A. UNTCH, D. VASILJEVIC, P. VITERBO, J. WOOLLEN, 2005: The ERA-40 re-analysis. – Quart. J. Roy. Meteor. Soc. **131**, 2961–3012.